Rajata Kumar Mansingh [1]
Raj Kishore Mishra [2]
Tapan Dash [1,3*]
Asis Mishra [4]
Surendra Kumar Biswal [3]

[1] Centurion University of Technology and Management, Odisha, INDIA
[2] Maharishi College of Natural Law, Saheed Nagar, Bhubaneswar, Odisha, INDIA
[3] International PranaGraf Mintech Research Centre (IGMRC), Bhubaneswar, Odisha, INDIA
[4] Guru Ghasidas Vishwavidyalaya Bilaspur (C. G.), Chhattisgarh, INDIA

* Corresponding author
Email: tapanphy@gmail.com

Graphene Reinforced BFO: New Nanocomposite for Multifunctional Applications for Future Technology

This research illustrated the effective synthesis of graphene (0.04 mol) reinforced BFO composite and assessed its spectroscopic properties for various important applications, including supercapacitors and photocatalytic activities. The Raman analysis revealed the presence of D, G, and 2D peaks in the graphene. The energy band gap was measured to be an impressive 1.61 eV. Functional groups associated with the graphene were identified through Fourier-transform infrared (FTIR) analysis. These characteristics, along with the results from transmission electron microscope (TEM) microstructural analysis, confirm the high quality of the few-layer (2-4) graphene. Graphene reinforcement significantly increases the BET surface area of BFO from 4.2 to 78 m^2/g. Remarkably, it also reduces the energy band gap of BFO from 2.62 to 1.68 eV upon adding graphene. The electrical conductivity of BFO has been evaluated at $4.2x10^{-4}$ S/cm. However, the conductivity value is projected to increase to 2.58 S/cm for our BFO/graphene (4 mol) composite.

Keywords: Graphene; BFO; Composites; Spectroscopic properties
Received: 4 June 2025; **Revised:** 31 August; **Accepted:** 7 September 2025

1. Introduction

Bismuth ferrite ($BiFeO_3$, BFO) is a significant multiferroic material that displays both ferroelectric and antiferromagnetic ordering at room temperature. This characteristic renders it an attractive option for advanced multifunctional devices, including sensors, memory devices, and spintronic components [1-3]. However, its practical applications are often limited by inherent drawbacks such as high leakage current, poor electrical conductivity, and structural instability [4,5]. To address these limitations, composite materials incorporating $BiFeO_3$ with conductive nanomaterials like graphene have emerged as a promising approach [5-7]. Graphene, a two-dimensional carbon nanomaterial known for its extraordinary electrical conductivity, mechanical strength, and large surface area [8,9], can significantly enhance the performance of $BiFeO_3$-based systems. When combined, $BiFeO_3$/graphene composites exhibit synergistic effects-graphene improves charge transport and can enhance mechanical properties, while $BiFeO_3$ retains its multiferroic nature, thereby broadening the functional capabilities of the composite.

The synthesis of bismuth ferrite/graphene ($BiFeO_3$/graphene) composites presents several significant challenges that affect the material's structural integrity and functional performance. Ensuring strong interfacial contact between $BiFeO_3$ nanoparticles and graphene sheets is crucial but difficult, as weak bonding can severely hinder charge transfer efficiency, which is vital for applications like photocatalysis and energy storage [6,7]. The tendency of $BiFeO_3$ nanoparticles to agglomerate further complicates uniform distribution on the graphene surface, leading to reduced active surface area and uneven composite morphology. Controlling the particle size and shape is also challenging yet essential, as these factors can directly influence the composite's magnetic, catalytic, and electrical properties. The powder metallurgy route presents a solid-state, scalable, and cost-effective method for synthesizing $BiFeO_3$/graphene composites. This technique involves blending, compacting, and sintering the constituent powders, offering precise control over the composite formation. Furthermore, powder metallurgy minimizes the degradation of graphene and prevents undesirable phase transitions in $BiFeO_3$, which are common at high temperatures in traditional synthesis methods.

This study focuses on the synthesis, spectroscopic, specific surface area and electrical conductivity of $BiFeO_3$/graphene composites prepared via powder metallurgy. The goal is to develop a composite material with enhanced properties suitable for advanced electronic and photocatalytic applications.

2. Experimental Part

The precursor powders are bismuth oxide (Bi_2O_3), ferric oxide (Fe_2O_3) and graphene. Bi_2O_3 with a purity of 99.9% and Fe_2O_3 with a purity of 99.8% were procured from Sigma-Aldrich. Graphene has been procured from the International PranaGraf Mintech

Research Centre (IGMRC) in Bhubaneswar, Odisha, India, characterized by a purity level greater than 99.98%, 2-4 number of layers and specific surface area of 550 m^2/g. The precursor powders were mixed mechanically in an appropriate stoichiometric ratio. In our earlier work we have studied the reinforcement effect of 0.02 mol of graphene in BFO by powder metallurgy route [10]. However, we couldn't successes in obtaining optimized nanocomposite of BFO/graphene. In this mixture, graphene of 0.04 mol was added and the final mixture was mixed with ethanol and ground mechanically in an agate mortar for about 3 hours to achieve a homogenous mixture. To develop homogeneous nanocomposites with minimized particle size from powder samples, they underwent mechanical grinding in a high-energy dry planetary ball mill. The ball milling was carried out in an argon atmosphere. Tungsten carbide balls, both 2 mm and 4 mm in equal amounts of 0.5 kg, served as the grinding media during this process. The milling continued for 5 hours, with samples positioned in two jars (jar volume-3000 cm^3) of the ball mill at a sample-to-ball ratio of 1:10. The planetary ball mill functioned at a speed of 300 rpm. After the milling process, the powder samples were removed from the jars. Following the ball milling, the samples were compacted at pressures of 100 MPa for 120 s in a 13 mm die. The compacted samples were then subjected to sintering in a regulated furnace within an argon environment at a temperature of 800°C for a duration of 3 hours.

The characteristics of reduced graphene oxide (rGO) and sintered materials have been examined utilizing characterization methods like particle size assessment via a laser scattering particle size distribution analyzer (LA-960V2, Horiba Scientific). The FTIR spectroscopy was performed using the NICOLET iS50 model, and TEM was conducted with the TECNAI G2 (200 kV) from FEI (Netherlands). Micro Raman spectroscopy was carried out with a Renishaw India Reflex (UK) spectrometer that employs an Ar^+ ion laser. Brunauer-Emmett-Teller (BET) analysis was completed using an automated gas sorption analyzer from Quantachrome instruments, along with UV-visible Diffuse Reflectance Spectroscopy (UV-Vis DRS) conducted with a Thermo Scientific Evolution 220 model. The electrical conductivity was assessed using a four-probe digital meter (multimeter Keithley 6221).

3. Results and Discussion

A comprehensive examination of graphene, utilized as a super-additive element to enhance the properties of the BFO matrix, is crucial and is thoroughly investigated in this research. The spectroscopic characteristics of graphene were assessed using FTIR spectroscopy, with the results presented in Fig. (1). The used graphene in this work has been prepared from high purity graphite by mechanical ball milling technique. This band at 1577 cm^{-1} (C-C stretching vibration mode) is important as it represents the skeletal vibrations of the carbon network in graphene The presence of this peak is reasonably sharp and distinct peak, which indicates the retention of sp^2 hybridized carbon network of graphitic domains even after following mechanical milling. The vibration band occurred at 1185 cm^{-1} (C-OH stretching vibration) indicates functional group associated with reduced nature of graphene. The presence of a strong and broad peak around 3404 cm^{-1} is characteristic of O-H stretching vibrations is due to deposition of surface moisture because of its exposure to open atmosphere. The FTIR findings are in good agreement with the spectroscopic behavior of graphene reported in the literature [11].

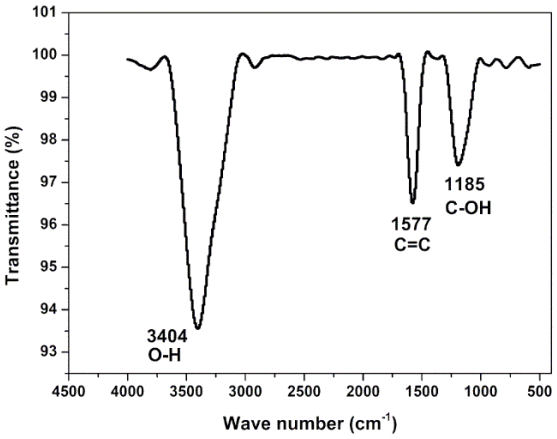

Fig. (1) FTIR spectrum of graphene

The TEM analysis of the graphene sample demonstrates its high transparency, which confirms the effective separation and exfoliation of its various layers (Fig. 2). The graphene sheets predominantly exhibit a flooded appearance. The thin, twisted structures are oriented randomly, with numerous thin layers interwoven with one another. The sheets of graphene are featuring scrolling at the edges.

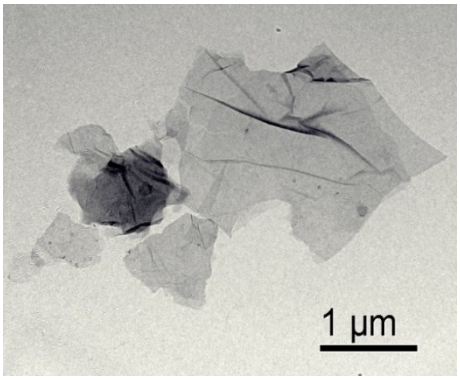

Fig. (2) TEM image of microstructural analysis of graphene

The median size variation (D50) of BFO and Al/graphene (0.04 mol) samples is measured using a laser particle size analyzer. It has been observed after the milling of 5 hours, it causes a shape decrease in particle size. There is a sharp decrease in particle size compared to the initial size of BFO (particle size ≤50 µm and BFO/graphene (particle size < 20 µm). In this work, we have obtained optimized particle size (D_{50}) for pure BFO and BFO/graphene as 90 and 42 nm, respectively, in mechanical milling. Hence, the addition of graphene is found to accelerate the milling process to reduce particle size. The micro Raman spectroscopy of graphene, BFO, and BFO/graphene composite are presented in Fig. (3). The micro Raman spectroscopy analysis of graphene reveals peaks corresponding to D (which is associated with the first disorder peak of graphite), G (resulting from sp^2 carbon within the graphite lattice), and 2D (linked to the stacking layers of graphene) at 1347, 1578, and 2689 cm^{-1}, respectively [11]. The intensity ratio of the 2D band to the G band is approximately 0.5. The 2D peak position is found to appear at a relatively lower Raman shift. The intensity of 2D and peak position are suggesting that the graphene consists of 2-4 graphene sheets [12,13]. This quality of graphene can play vidal role in the graphene-reinforced BFO composite. BFO shows peaks at 65, 220, 287, 401, 495, 601, 657, 816, and 1303 cm^{-1}, and such type of results were obtained in the literature [6]. Graphene-reinforced BFO shows peaks for BFO and peaks for graphene. We have been observed for BFO/graphene (0.04 mol) composite that while the peaks of BFO are slightly shifting to higher Raman shift, the peaks of graphene are shifted to lower Raman shift. The intensity of peaks related to BFO are reduced after graphene reinforcement to it and some peaks like 65 and 816 cm^{-1} are completely removed. We also observed there is reduction in linewidth of the peaks appeared for BFO and graphene in the composite. While D peak intensity increases, G peak and 2D peak show reduced peak intensity in compared to pure graphene. Such type of spectroscopic behaviour may be caused due to lattice interaction between BFO and graphene. The activation of Van der Waals forces is common in graphene, which facilitates close contact but weak binding with BFO. The lattice interaction may be also developed due to interactions between graphene's π-electrons and Fe 3d orbitals of BFO, which possibly leading to charge transfer. There might be also electrostatic interactions or weak chemisorption between functional groups of C–OH of graphene and BFO surface atoms. There is almost no possibility of strong covalent bonding otherwise it would cause more pronounced structural or spectral changes. Decreased peak intensity of graphene 2D band indicates π–π stacking disruption or electron transfer. The D-band intensity increases relative to the G-band suggests defect generation due to interaction.

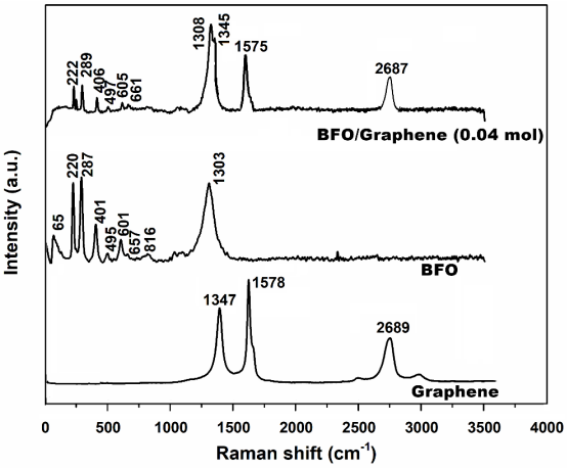

Fig. (3) Micro Raman analysis results of graphene, BFO and BFO/graphene (0.04 mol) composite

The UV-Vis DRS spectrum of graphene was acquired to evaluate the optical energy gap. The energy band gap of graphene was determined utilizing the Kubelka–Munk function [14] in relation to the energy of light. The calculated energy band gap is 1.61 eV, as depicted in Fig. (4). Generally, the energy band gap of graphene is about 2.0 eV. But in our case, the value is less than 2.0 eV. The relatively low band gap is very important for modifying the spectroscopic behaviour of BFO, especially in making the composite ready for supercapacitor applications. The graphene addition is found to significantly reduce the band gap energy for BFO. BFO shows an energy band gap of 2.62 eV, whereas, upon addition of graphene in BFO, it lowers the band gap to 1.68 eV, which is a significant achievement in the study and found to be lower than the value reported in the literature [6]. The graphene used in the study has a BET SA of 550 m^2/g. The specific surface area of BFO was determined by the BET technique and was found 4.2 m^2/g. The graphene reinforcement is found to enhance the specific surface area to 78 m^2/g, which is relatively higher than the value reported in the literature [15]. The electrical conductivity of BFO was measured at $4.2x10^{-4}$ S/cm. The conductivity value is found to increase to 2.58 S/cm for our BFO/graphene (4 mol) composite. The above increase in electrical conductivity measured for our BFO/graphene (4 mol) composite is significantly higher than that of BFO/rGO (10-30 % rGO) composites which showed electrical conductivity in the range of 4.96×10^{-2}-1.78 S/cm [5]. The enhancement in electrical conductivity from 4.2×10^{-4} S/cm (BFO) to 2.58 S/cm (BFO/graphene (4 mol) composite) is remarkable. The synthesis method (powder metallurgy) and the graphene-BFO interface play synergistic roles in achieving this result. The effective powder metallurgy route promotes homogeneous dispersion of graphene within the BFO matrix which develops well-connected

conductive pathways across the entire composite. Graphene's π-electron structure creates faster charge transfer medium. The high surface area of graphene stimulates better interfacial adhesion to BFO particles. Graphene sheets develops a well-bonded contact allows for electron hopping or tunneling between BFO particles. Better electron mobility is also facilitated by grain-to-grain contact caused by the optimized compaction and sintering processes used in this work.

The above-achieved spectroscopic behavior along the specific surface area and electrical conductivity of the BFO/graphene composite makes it a very suitable composite for multifunctional applications including supercapacitor and photocatalytic industrial applications.

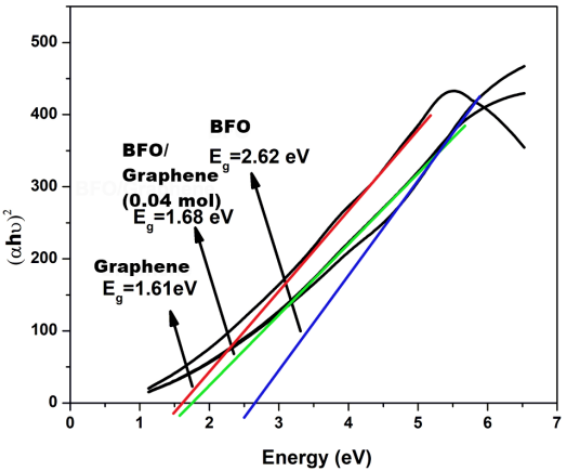

Fig. (4) UV-visible DRS analysis results of graphene, BFO and BFO/graphene (0.04 mol) composite

4. Conclusions

The study demonstrates the successful synthesis of graphene (0.04 mol) reinforced BFO composite and its spectroscopic behavior. The graphene shows D, G, and 2D peaks in Raman analysis, with a 1.61 eV energy band gap. FTIR and TEM microstructural results further confirm the quality of the graphene which has approximately 2-4 sheets in its nanostructure. Graphene reinforcement improves nanocomposite formation kinetics and particle size reduction compared to pure BFO. It enhances BET SA of BFO from 4.2 to 78 m^2/g and reduces the energy band gap from 2.62 to 1.68 eV. The electrical conductivity of BFO has been assessed at $4.2x10^{-4}$ S/cm. Furthermore, the conductivity value is determined to enhance to 2.58 S/cm for our BFO/graphene (4 mol) composite. These properties could lead to significant industrial applications of such composite in the field of supercapacitors and photocatalytic.

References

[1] Q. Zhang, D. Sando and V. Nagarajan, "Chemical route derived bismuth ferrite thin films and nanomaterials", *J. Mater. Chem. C.,* 4 (2016) 4092-124.

[2] R.K. Mansingh, R.K. Mishra and T. Dash, "Modifying $BiFeO_3$ (BFO) for multifunctional applications- A review", *AIP Conf. Proc.*, 2417 (2021) 1-7.

[3] N. Wang et al., "Structure, performance, and application of $BiFeO_3$ nanomaterials", *Nano-Micro Lett.,* 81 (2020) 1-23.

[4] S. Chauhan et al., "Ca–Li substitution driven structural, dynamics of electron density, magnetic and optical properties of $BiFeO_3$ nanoparticles", *J. Alloy. Compd.,* 811 (2019) 151965.

[5] J. Liao, M. Ye and A. Han, "Synthesis and characterization of $BiFeO_3$/RGO composites for promising microwave absorption materials", *J. Mater. Sci.: Mater. Electron.,* 31 (2020) 6988-6997.

[6] M. Ghorbani et al., "Modified $BiFeO_3$/rGO nanocomposite by controlled synthesis to enhance adsorption and visible-light photocatalytic activity", *J. Mater. Res. Technol.,* 22 (2023) 1250-1267.

[7] A. Soam et al., "Power performance of BFO-graphene composite electrodes based supercapacitor", *Mater. Res. Exp.*, 6 (2018) 1-14.

[8] B.B. Palei, T. Dash and SK Biswal, "Preparation of graphene reinforced aluminium composites: investigation of microstructural, electrical conductivity and microhardness behaviour", *Int. J. Mater. Prod. Technol*., 62 (2021) 49-64.

[9] T. Dash et al., "Study on microstructural influence of graphene on synthesis of $BaTiO_3$", *Mater. Today Proc.*, 43 (2021) 447-450.

[10] T. Dash et al., "Retaining graphene structure in the synthesis of its composite with $BiFeO_3$", *Mater. Today Proc*., 43 (2021) 216-219.

[11] S. Dhar et al., "Study on the microstructure and microhardness behavior of reduced graphene oxide reinforced alumina nanocomposites", *J. Mater. Eng. Perform.,* 33 (2024) 5446-5457.

[12] V. Kumar et al., "Estimation of number of graphene layers using different methods: A focused review", *Materials (Basel)*, 14 (2021) 1–22.

[13] B.B. Nayak et al., "Growth of carbon nanotubes in arc plasma treated graphite disc: microstructural characterization and electrical conductivity study", *Appl. Phys. A*, 124 (2018) 1–9.

[14] A.E. Morales, E.S. Mora and U. Pal, "Use of diffuse reflectance spectroscopy for optical characterization of un-supported nanostructures", *Rev. Mex. Fis.*, 53 (2006) 18–22.

[15] S. Rizwan and S. Fatima, "Bismuth ferrites/graphene nanoplatelets nanohybrids for efficient organic dye removal", edited by Y. Zhou, F. Dong and S. Jin, "Bismuth - advanced applications and defects characterization", InTech Open (2018), doi: 10.5772/intechopen.71174.

